Electronic Supplementary Material (ESI) for Polymer Chemistry.

Supporting Information

Photocycloreversions within Single Polymer Chains

Modan Liu, Wolfgang Wenzel and Hendrik Frisch

Contents

1. Additional experiments

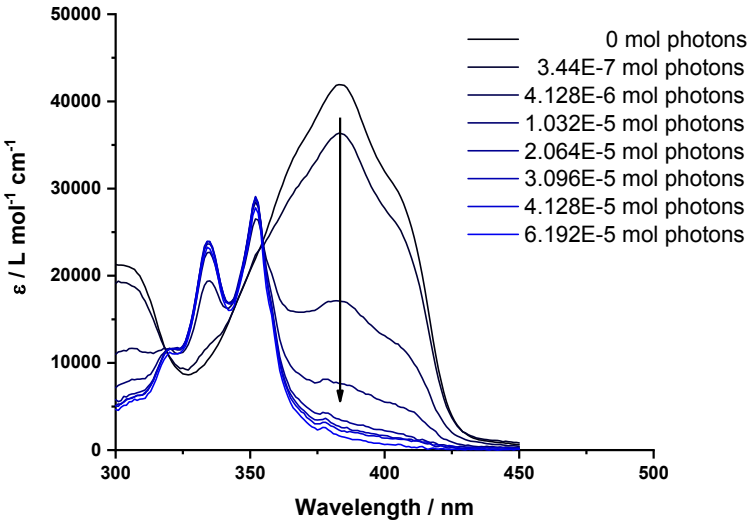

Figure S1: UV/vis spectra of **P1'** after irradiation at λ = 430 nm.

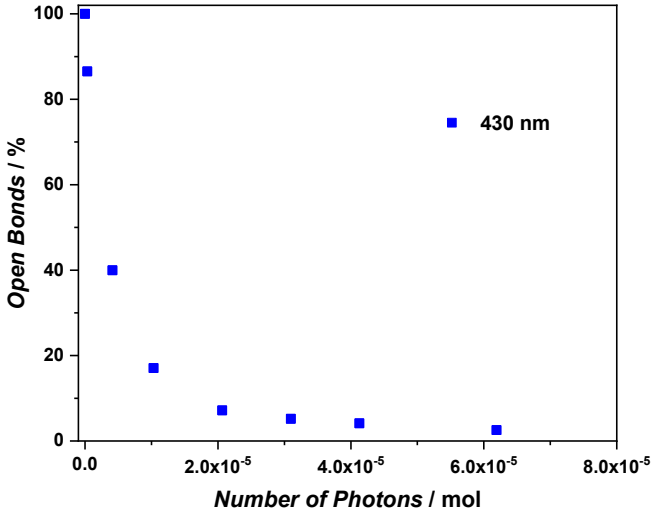

Figure S2: Styrylpyrene cycloreversion yield within **P1'** as a function of the number of incident photons at λ = 430 nm calculated from the UV/vis spectra.

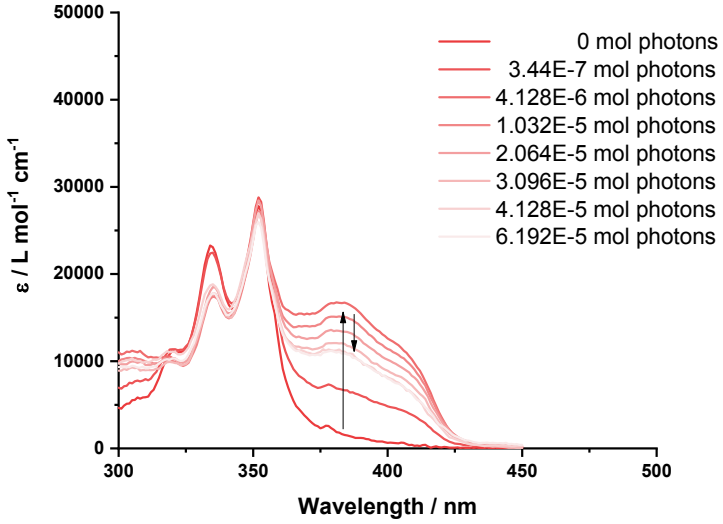

Figure S3: UV/vis spectra of **SCNP1'** after irradiation at λ = 330 nm.

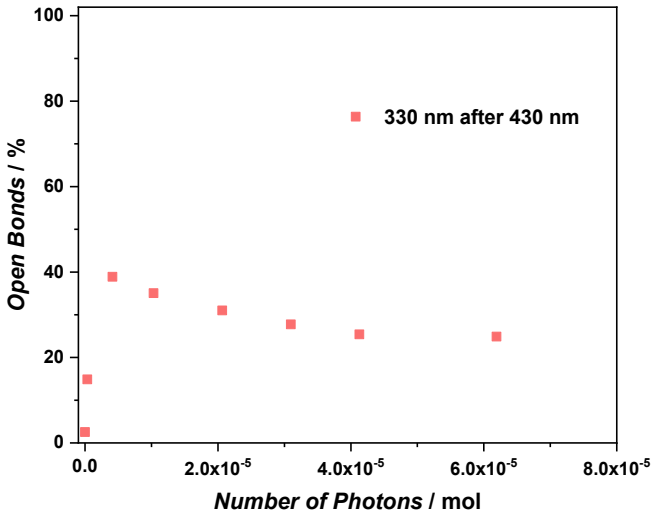

Figure S4: Styrylpyrene cycloreversion yield within **SCNP1'** as a function of the number of incident photons at λ = 330 nm calculated from the UV/vis spectra.

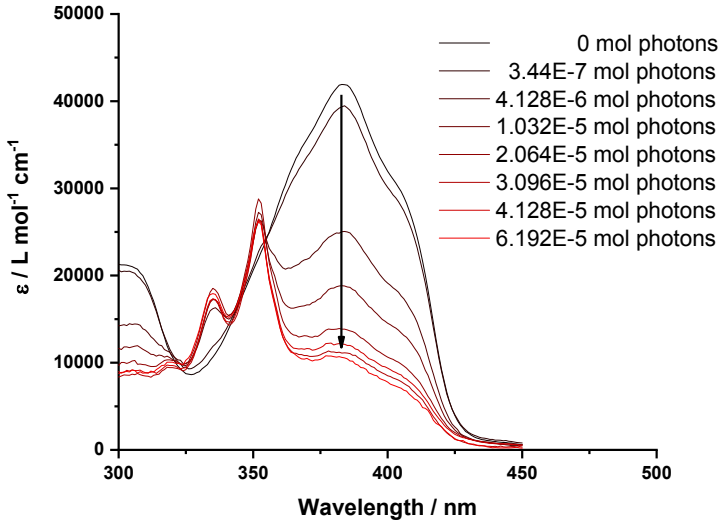

Figure S5: UV/vis spectra of **P1'** after irradiation at λ = 330 nm.

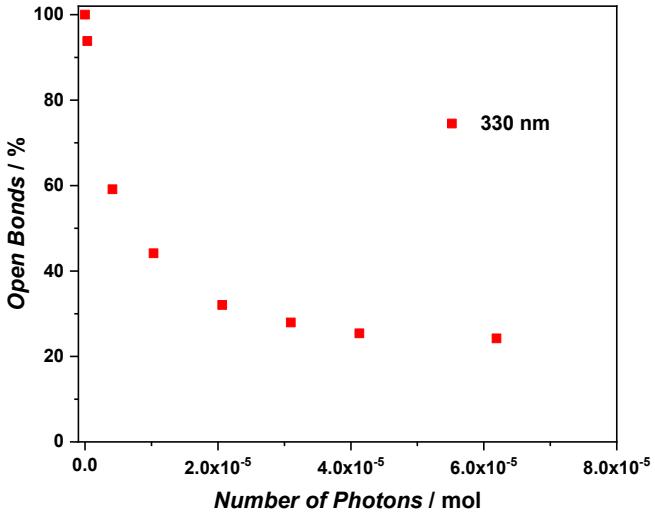

Figure S6: Styrylpyrene cycloreversion yield within **P1'** as a function of the number of incident photons at λ = 330 nm calculated from the UV/vis spectra.

2. Calculation of photoreactive groups per polymer chain of P1'

Following a previously published procedure[1] based on the percentage of styrylpyrene containing monomer **M1** in **P1'** obtained from the ^{1}H-NMR spectra and the $\bar{M}_n$ obtained from the SEC, the average number of **M1** units and MMA monomers per polymer chain were calculated as follows:

$$n(M1) = n(monomers) \bullet X(M1)$$

$$n(MMA) = n(monomers) \bullet X(MMA)$$

With the average number of monomers per polymer chain $n(monomers)$:

$$n(monomers) = \frac{\bar{M}_n\ (Polymer)}{M_{Average}(monomer)}$$

With the average monomer mass ($M_{Average}$):

$$M_{Average} = X(M1) \bullet M(M1) + X(MMA) \bullet M(MMA)$$

Resulting in the following formula:

$$n(M1) = \left(\frac{\bar{M}_n\ (Polymer)}{X(M1) \bullet M(M1) + X(MMA) \bullet M(MMA)}\right) \bullet X(M1)$$

For **P1'** this leads to:

$$n(M1) = \left(\frac{19{,}300\ \ g\ mol^{-1}}{0.3 \bullet 533\ \ g\ mol^{-1} + 0.7 \bullet 100\ \ g\ mol^{-1}}\right) \bullet 0.3 = 25$$

$$n(MMA) = \left(\frac{19{,}300\ \ g\ mol^{-1}}{0.3 \bullet 533\ \ g\ mol^{-1} + 0.7 \bullet 100\ \ g\ mol^{-1}}\right) \bullet 0.6 = 58$$

3. Experimental details

3.1 THF-SEC

The SEC measurements were conducted on a PSS SECurity2 system consisting of a PSS SECurity Degasser, PSS SECurity TCC6000 Column Oven (35 °C), PSS SDV Column Set (8 x 150 mm 5 µm Precolumn, 8 x 300 mm 5 µm Analytical Columns, 100000 Å, 1000 Å and 100 Å) and an Agilent 1260 Infinity Isocratic Pump, Agilent 1260 Infinity Standard Autosampler, Agilent 1260 Infinity Diode Array and Multiple Wavelength Detector (A: 254 nm, B: 360 nm), Agilent 1260 Infinity Refractive Index Detector (35 °C). HPLC grade THF, stabilized with BHT, is used as eluent at a flow rate of 1 mL·min^{-1}. Narrow disperse linear poly(methyl methacrylate) ($\bar{M}_n$: 202 g·mol-1 to 2.2x106 g·mol^{-1}) standards (PSS ReadyCal) were used as calibrants. All samples were passed over 0.22 µm PTFE membrane filters. Molecular weight and dispersity analysis was performed in PSS WinGPC UniChrom software (version 8.2).

3.2 1D NMR Measurements

^{1}H- and ^{13}C-spectra were recorded on a *Bruker* System 600 Ascend LH, equipped with a BBO-Probe (5 mm) with z-gradient (^{1}H: 600.13 MHz, ^{13}C: 150.90 MHz,). All measurements were

carried out in deuterated solvents. The chemical shift (δ) is recorded in parts per million (ppm) and relative to the residual solvent protons.[2] The measured coupling constants were calculated in Hertz (Hz). To analyze the spectra the software MESTRENOVA 11.0 was used. The signals were quoted as follows: s = singlet, bs = broad singlet, d = doublet, t = triplet, dd = doublet of doublets and m = multiplet.

3.3 UV-VIS Spectroscopy

UV/vis spectra were recorded on a *Shimadzu* UV-2700 spectrophotometer equipped with a CPS-100 electronic temperature control cell positioner. Samples were prepared in THF and measured in *Hellma Analytics* quartz high precision cells with a path length of 10 mm at ambient temperature.

3.1 Experiments using laser irradiation

Tunable laser experiments with a constant photon count at varied wavelengths were carried out according to a procedure that was published earlier by us: [3–5]

"An *Innolas* Tunable Laser System SpitLight 600 OPO was applied as light source. An optical parametric oscillator (OPO) was pumped with a diode pumped Nd:YAG laser (repetition rate 100 Hz). The energy of the laser pulses was downregulated by an attenuator (polarizer). The beam is redirected into the vertical cylindrical hole of a custom-made sample holder, which contains the samples during the experiments (refer to Scheme 1). These glass vials are crimped 0.7 mL vials by LLG Labware, Lab Logistic Group GmbH (Art. Nr. 4-008202). The energy of the incident laser pulses was measured by an Energy Max PC power meter (Coherent) directly above the sample holder. Prism and sample holder are positioned in a way that the complete diameter of the hole of the sample holder is covered by the incident laser beam." (Adapted from previous publications[3–5])

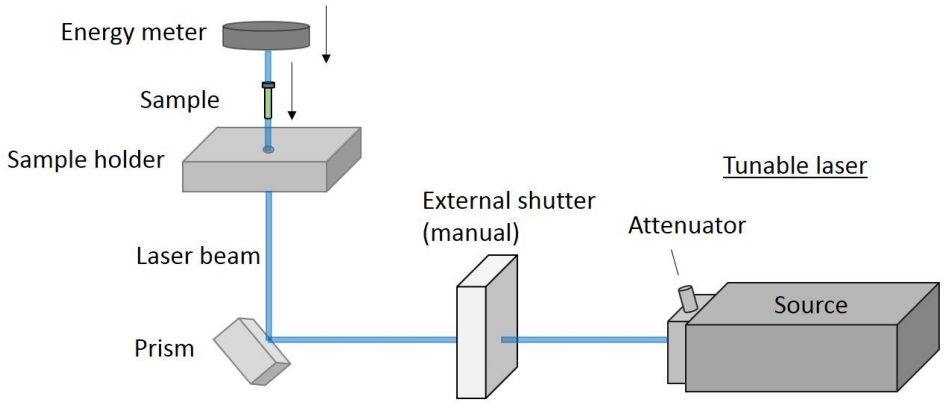

Scheme S1. Experimental setup for tunable laser experiments. The energy output is regulated with the attenuator and controlled with the energy meter (setup without sample). Measurement of energy and irradiation of samples cannot be done simultaneously. An individual setting of the attenuator is necessary before each irradiation experiment. (Adapted from previous publications[3–5])

3.1.1 Control over the incident number of photons in a tunable laser experiment[6]

The number of photons n_p ([n_p] = mol) that a monochromatic laser pulse contains can be calculated by application of the Planck-Einstein relation from the energy of the pulse E_{pulse}, the incident wavelength λ, Planck's constant h and the speed of light c:

$$n_p = \frac{E_{pulse}\ \lambda}{h\ c\ N_A}$$

If the absorption of the glass vial and the extent of reflection and scattering at the vial at the respectively relevant wavelength is known, a target energy value can be calculated that must be reached during the above described measurement to guarantee that the desired number of photons penetrates the sample solution during the subsequent irradiation. The wavelength dependent transmittance of the glass vials was determined experimentally using the above setup. Three glass vials were randomly selected as calibration vials. For varying wavelengths and in each case at a constant power output of the laser the energy was measured both with and without the calibration vials fitted into the sample holder. The top parts of these vials were cut off to minimize errors in the procedure, since only the bottom and sides of the glass vials would contribute significantly to the reduction of the photon flux that enters the solution.

The measured energy per pulse without a calibration vial in the sample holder is denoted as E_0 and the measured energy per pulse with a calibration vial in the sample holder as E_n. The transmittance was calculated as the ratio of E_n to E_0. The average transmittance over the measurements of the three vials (T_λ) was plotted together with the respective error (compare Figure S):

$$T_\lambda = \frac{E_n}{E_0}$$

The target energy per pulse E_0 can be calculated directly from the wavelength λ, the number of pulses k, the transmittance of the glass vial at the respective wavelength T_λ and the desired total photon count n_p:

$$E_0 = \frac{n_p\, N_A\, h\, c}{k\, T_\lambda\, \lambda}$$

By controlling the target E_0 at the respective wavelength, the number of photons that penetrate each sample solution of one set of experiments as described in the following subsections was guaranteed to be identical despite irradiation at different wavelengths.

3.1.2 Transmittance of the glass vials[6]

As previously described,[6] the transmittance of the glass vials that were used for photoreactions with the tunable laser system was determined as follows. Measurement of the energy of laser pulses at a constant energy output was carried out directly above the sample holder first without a glass vial in the sample holder and subsequently with an empty glass vial in the sample holder. The headspace section of the glass vials was removed for these measurements to detect only the absorbance of the bottom of the vial (refer to Figure S12).

The described procedure was performed for three individual glass vials to account for variabilities between the vials. The obtained averaged values are listed in Table S1.

Figure S7*:* Left: uncrimped vial; right: vial after removal of the headspace section.

Table S1. *Transmittance of the glass vials used for the laser experiments.*

λ / nm	T_λ / %	Mean Deviation / %
285	13.3	1.3
295	28.2	2.6
305	33.0	3.2
315	43.9	4.3
325	49.1	2.7
335	55.1	3.5
345	55.7	2.4
355	57.5	3.3
365	60.3	4.3
375	61.0	3.6
385	61.1	3.2
395	62.8	3.6
405	62.4	4.6
415	64.8	1.9
425	65.0	2.6
435	67.5	2.0

445	65.9	3.0
455	64.5	2.4
465	67.7	3.1
475	68.8	3.0
485	65.6	3.2
495	65.9	4.0

The data was subsequently fitted to obtain values for the wavelengths that have not been measured during the calibration process (refer to Figure S13).

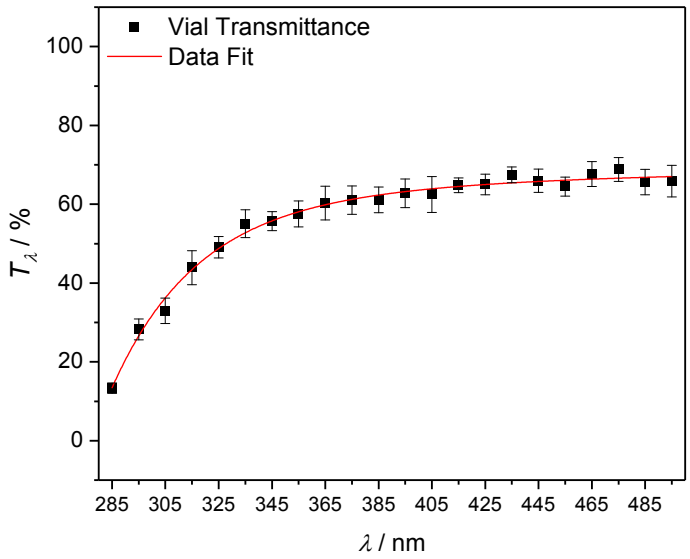

Figure S8. Calibration of the glass vial transmittance including a fit to obtain the values that were not determined experimentally.

$$T_\lambda = -227740.83 * e^{\frac{\lambda}{-30.79906}} - 233360.80115 * e^{\frac{\lambda}{-30.79938}} - 119.37996 * e^{\frac{\lambda}{-122.06264}}$$

3.1.3 Irradiation procedure with control over the photon count[6]

Prior to each irradiation, the respective solution was deoxygenated by purging with a stream of argon for five minutes. The tunable laser, including the pump source, was started and the internal shutter was opened several minutes before irradiation to allow the energy output of the laser to stabilize. The direction of the beam was controlled by adjusting the orientation of

the prism. The entire cross-sectional area of the sample is irradiated by the laser beam. The intensity of the beam was monitored and adjusted with the built-in polarizer (attenuator). A calculated target energy value was set, which enables the irradiation with the desired number of photons during the irradiation time.

4. Synthetic procedures

4.1 Materials

Unless stated otherwise, all chemicals and solvents were used as received from the supplier without further purification.

2-cyanopropan-2-yl benzodithioate (Sigma-Aldrich), methyl methacrylate (Sigma Aldrich, after passing through a short plug of basic alumina), AIBN (Sigma-Aldrich, recrystallized), DCM (Thermo Fisher Scientific, after drying and purification with SP-1 Stand Alone Solvent Purification System LC Technology Solutions Inc.), THF (Thermo Fisher Scientific), toluene (Thermo Fisher Scientific, after drying and purification with SP-1 Stand Alone Solvent Purification System LC Technology Solutions Inc.), hexanes (Thermo Fisher Scientific), methanol (Thermo Fisher Scientific), chloroform-d_1 (Sigma-Aldrich). **M1** was synthesized according to a literature known procedure.[1]

4.2 iSynthesis

4.2.1 P1

P1 was synthesized as previously described and used without modifications.[1]

4.2.2 P1'

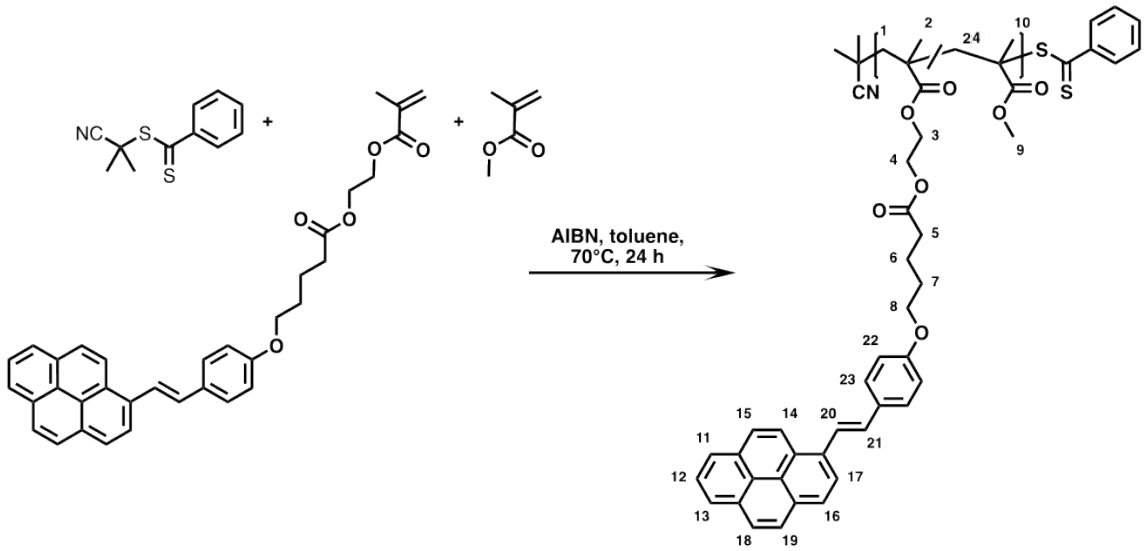

The synthesis of **P1'** was adopted from a previously described procedure. 2-cyanopropan-2-yl benzodithioate (0.3 mg, 10 μmol, 1.0 eq.), methyl methacrylate (33.5 mg, 258 μmol, 240.0 eq.), 2-(methacryloyloxy)ethyl(E)-5-(4-(2-(pyren-1-yl)vinyl)phenoxy)pentanoate (**M1**)[1] (38.9 mg, 73 μmol, 68.0 eq.) and AIBN (0.035 mg, 0.2 μmol, 0.2 eq.) were dissolved in 100 μL toluene. The reaction mixture was purged with argon for 10 min and afterwards stirred at 70 °C over night. The reaction mixture was precipitated out of cold methanol and the precipitate purified via preparative size exclusion chromatography to removed unreacted monomer (Sephadex® LH 20, THF). The polymer was dissolved in an excess of THF, the solution purged with air and stirred overnight in an open flask to remove remaining RAFT end groups. The residue was redissolved in THF followed by precipitation out of cold *n*-hexane.

Isolated yield: 10 mg.

SEC (PMMA cal.): $\bar{M}_n$ = 19,300 g mol^{-1}.

^{1}H-NMR (600 MHz, $CDCl_3$) δ (^{1}H) = 8.45 – 7.76 (m, CH-11-19, 21), 7.60 – 7.35 (m, CH-23), 7.26 – 7.08 (m, CH-20), 6.90 – 6.73 (m, CH-22), 4.31 – 3.82 (m, CH_2-4,3,8), 3.49 (bs, CH_3-9), 2.43 – 2.30 (m, CH_2-5), 2.03 – 0.65 (m, backbone).

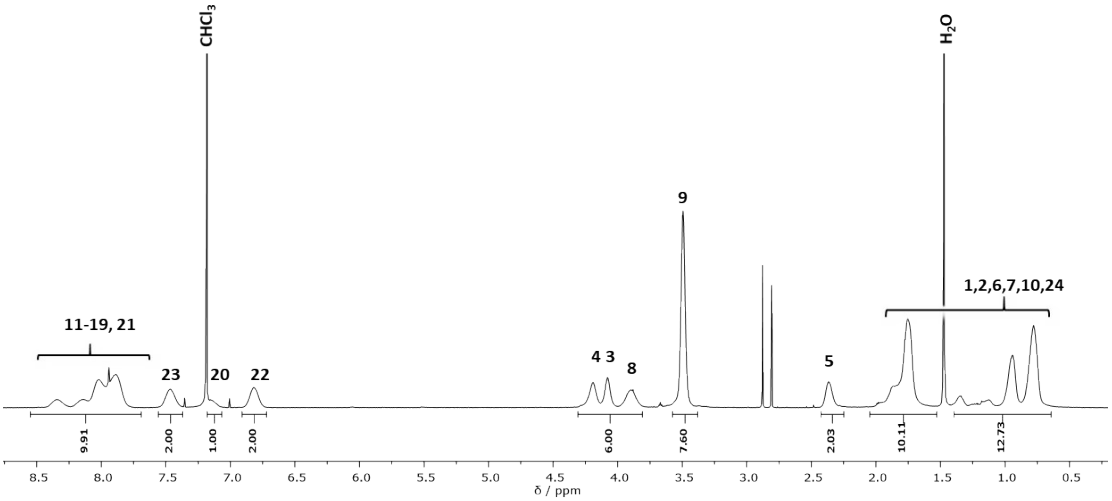

Figure S9: ^{1}H-NMR spectrum of **P1'** in $CDCl_3$.

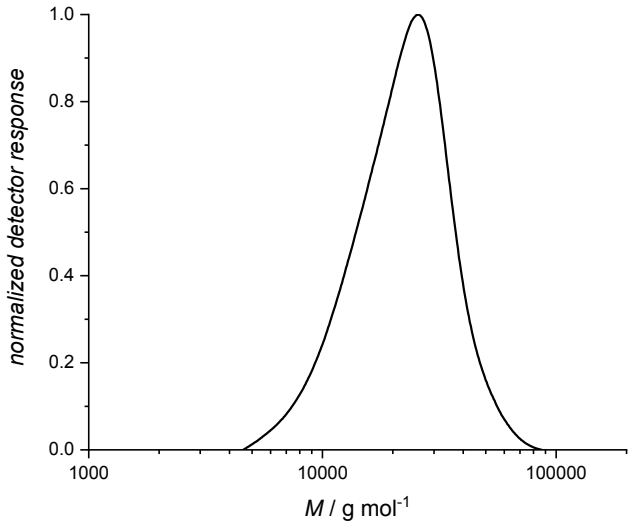

Figure S10: SEC trace of **P1'** in THF using a PMMA calibration.

5. Simulations

5.1 Coarse-grained molecular dynamics model

We use a dissipative particle dynamics (DPD)[7] model, where the polymer-solvent system is coarse-grained into subgroups which are represented by individual beads. Interaction among DPD beads for both the SCNP and the solvent follow a pair-wise scheme in which 3 force components are additive:

$F_{DPD} = F_{conservative} + F_{dissipative} + F_{random}$

The conservative component implements a short-range soft repulsion, models the mutual solubility among monomer-monomer, monomer-solvent, and solvent-solvent species. The conservative force [8] is represented as:

$F_{conservative} = a_{ij}\omega(r_{ij})$

$\omega(r_{ij}) = 1 - r_{ij}/r_{cutoff}$

where r_{ij} is the distance between DPD beads and a_{ij} as the repulsion amplitude is scaled via the scaling function $\omega(r_{ij})$ to be linearly vanishing towards cut-off distance r_{cutoff}. In the SCNP model the cut-off distance is routinely taken as unit DPD length L_{DPD}.

In thermal equilibrium the dissipative component of DPD, formulated as:

$F_{dissipative} = -\gamma\omega(r_{ij})(\hat{r}_{ij} \cdot \vec{v}_{ij})$

is correlated via the fluctuation-dissipation theorem with the random force component:

$F_{random} = \sigma\omega(r_{ij})\theta/\sqrt{\Delta t}$

where the friction coefficient γ and random force term σ are coupled, such that $\sigma = \sqrt{2\gamma k_B T}$. Here k_B is the Boltzmann constant and T the temperature[7]. Dissipative and random forces work together as a MD thermostat for temperature regulation and characterize the diffusion timescale. In the MD simulation, we sample the random variable θ as uniformly distributed. Due to comparable small sizes and mass of the DPD subgroups, the friction coefficients γ across all species are taken to be identical with a value of 4.5 following reference[9] for a generic fluid-like characterization. From the reference, it is shown for a large enough number density of $\rho > 3{L_{DPD}}^{-3}$, the hydrodynamic boundary for the DPD fluid beads is invariant for $\gamma_{DPD} > 5\sqrt{m/\varepsilon_{DPD}}/L_{DPD}$, where the DPD energy unit $\varepsilon_{DPD} = k_B T$, and m the masses of DPD subgroups.[9]

The grouping scheme, shown in Fig. S11, ascertains that the molecular weights and friction coefficients are comparable across all DPD species to result in consistent in diffusion timescales and convergence towards thermal equilibration. The styrylpyrene complex classed as DPD types 3'-4-3 is dissected due to bulkiness compared with the MMA along with taking the consideration of representing the geometry of styrylpyrene as head section, crosslinking site, and tail section. While the photodimerization site

which resides on the C=C double bond shared between DPD types 3' and 4 is transferred solely upon type 4, the disection scheme assures that the masses of 3' and 3 are symmetric, henceforth the geometry conservation and the orientation dependence of the reduced styrylpyrene complex is orthogonally parameterized in FENE bonds rather than DPD.

FENE bonds interlinks DPD beads within the polymer chain via the potential[10]:

$$E_{FENE} = -Kr_{max}{}^{2} ln\left[1 - \frac{(r_{mn} - \delta)^2}{r_{max}{}^{2}}\right],$$

so that for small bond stretching of r_{mn} the bonding potential reduces to the standard harmonic form while for large bond extension r_{max} the length is bounded to preserve the molecular geometry. In our simulation the parameterization of FENE bonds for bond strengths K, balance lengths δ, and maximum bond lengths r_{max} are chosen such that the vibrational modes are consistent with the DPD timescale. The details of the FENE parameterization can be found in Table S3.

To prevent bond crossing in the DPD-FENE model, a segmental repulsive potential[11] is also introduced as:

$$F_{SRP} = C(1 - r_{uv}/r_{cutoff-SRP}),$$

where C correspond to maximum repulsion between bonds, where the cut-off follows DPD linear scaling form. The SRP parameters are chosen as $C = 8.0\varepsilon_{DPD}$, $r_{cutoff-SRP} = 0.25L_{DPD}$.

The CG DPD-FENE SRP scheme employs 5 types of units as illustrated in Fig. S11. This subdivision of the molecules is motivated by the fact that the units in the DPD simulation must have roughly the same size in order to produce the same diffusion dynamics and reactive units must be identifiable in the simulation. Parameterization details are listed in Table S2.

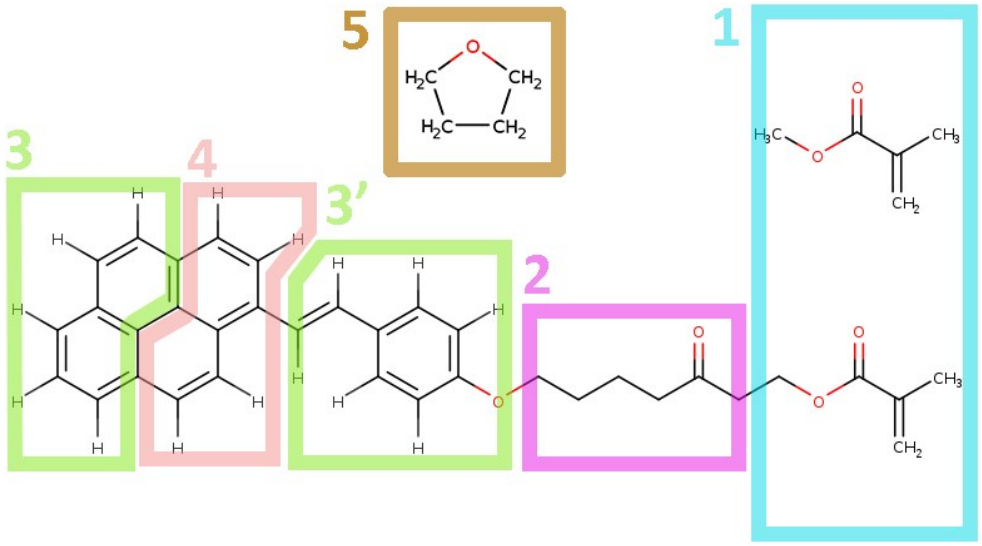

Figure S11. Coarse-graining scheme of **P1** in THF solvent, where the molecule is subdivided into units of different types. MMA occurs both in photoreactive and non-photoreactive monomers (unit type 1). Styrylpyrene containing monomer, designated as **M1**, is subdivided into an intermediate linker (unit type 2), which connects the MMA unit to the styrylpyrene unit (units types 3, 3' and 4). The photodimerization reaction occurs on the double bond connecting the head section of unit 3' and unit 4; in the CG model crosslinking is represented by a bond between two units of type 4 DPD beads. THF solvent molecules are represented as units of type 5.

5.2 CGMD parameterization

Table S2. Simulation parameters for the DPD-FENE SRP CGMD. Corresponding units are derived from reduced units in coarse grained DPD scheme where $L_{DPD} = 1.0$ nm, $m_{DPD} = 100$ Da, $\varepsilon_{DPD} = k_B T = 4.1416^{-21}$ J at 300K.

Mass of DPD units	
1 base	***1.001170***
2 monolink towards styrylpyrene	***1.150000***
3(3') styrylpyrene ring compound	***1.020000***
4 styrylpyrene ring compound, crosslink site	***1.000000***
5 THF	***0.721070***

Pair interactions	***DPD conservative A***	***DPD dissipative gamma***	***DPD cut-off R_cutoff***
1-1	***36.0***	***4.5***	***1.0***
1-2	***25.0***	***4.5***	***1.0***
1-3	***60.0***	***4.5***	***1.0***
1-4	***60.0***	***4.5***	***1.0***
1-5	***15.0***	***4.5***	***1.0***
2-2	***25.0***	***4.5***	***1.0***
2-3	***25.0***	***4.5***	***1.0***

2-4	***25.0***	***4.5***	***1.0***
2-5	***15.0***	***4.5***	***1.0***
3-3	***60.0***	***4.5***	***1.0***
3-4	***60.0***	***4.5***	***1.0***
3-5	***15.0***	***4.5***	***1.0***
4-4	***60.0***	***4.5***	***1.0***
4-5	***15.0***	***4.5***	***1.0***
5-5	***32.0***	***4.5***	***1.0***
Pseudo atom	***C***	***R_cutoff***	
SRP	***8.0***	***0.25***	

FENE bonds	***K***	***R_0***	***delta***
1-1 backbone	***24.0***	***1.5***	***0.6***
1-2	***5.0***	***2.5***	***0.8***
2-3	***5.0***	***2.5***	***0.8***
3-4	***40.0***	***1.5***	***0.6***
4-4 crosslink	***30.0***	***1.5***	***0.6***

Angles harmonic	***K***	***Theta0***
1-1-1 base	***1.4***	***109.2***
1-1-2	***1.4***	***109.2***
1-2-3	***1.4***	***109.2***
2-3-4	***1.0***	***120***
3-4-3	***1.0***	***120***
3-4-4 crosslink	***2.0***	***90***

5.3 Stochastic bond recombination

For irreversible SCNP folding induced by blue light, the bond formation rate is derived from photostationary state in Fig. 2c. For reversible SCNP folding induced by UV light, relative scales between bond formation and fission are derived from the photostationary state in Fig. 2f. The absolute bond formation rate is fitted to intermittent increase in the ratio of open bonds for SCNP1@330nm in Fig. 2c.

The sampling rate of bond recombination, i.e. the ratio between chemical reaction timescale and thermodynamic diffusion timescale, is scalable for folding with only blue or UV light. In exclusive blue light or UV light folding, a greater sampling rate, i.e. more frequent bond recombination events, can be offset by a lower local reaction probability following Bayesian rules, leading to invariant results. Taking the sampling rate to be ranging from 1 reaction attempted per 1e2$^{\tau_{DPD}}$to per 1e4$^{\tau_{DPD}}$, the dimerization rations with exclusive blue light and UV light exposure decrease monotonically, resulting in a consistent dynamic balance in the long-time limit. However, for dynamic partial unfolding in the case of SCNP1 subjected to 330nm light, the intermittent overly unfolding cannot be observed in the limit of very high sampling

rate, e.g. 1 reaction per τ_{DPD}. This observation indicates that a large enough separation of timescales is crucial to be able to describe the intermittent state, as diffusion must be a faster process than chemical reactions. This timescale separation reflects the fact photodimerization occurs under constrained conditions as styrylpyrene, which is bulky compared to the MMA base unit in the polymer, must exhibit good alignment before the bond is formed. Here in the simulation, the sampling rate is set to 1/1e2τ_{DPD}. The parameterization of bond recombination is shown in Table S3.

Table S3. Blue light (λ = 430 nm) induced crosslinking is parameterized in MD with solely bond formation rate, whereas UV light (λ = 330 nm) induced reversible reaction is characterized by both bond formation rates and bond fission rates.

Photochemical reaction	***Bond formation rate***	***Bond fission rate***
Irreversible	***0.2057 / 1e2τ_{DPD}***	***0***
Reversible	***0.6127 / 1e2τ_{DPD}***	***0.00035 / 1e2τ_{DPD}***

5.4 MD protocol

MD simulations are performed with LAMMPS software package[12]. Polymer systems **P1** and **P1'** are prepared in fixed lengths of 61 units and 83 units while the ratio of styrylpyrene-containing M1 monomers follow Gaussian distribution centered at 28% and 30% respectively to replicate photoreactive unit number distributions in the experiment. Corresponding to the 3 experimental protocols of blue laser exposure, UV laser exposure, and the subsequent blue-UV exposure, simulations are performed with respective rates. Dimerization ratios and radius of gyration are measured from simulations and are compared against UV/vis and SEC measurements in experiment.

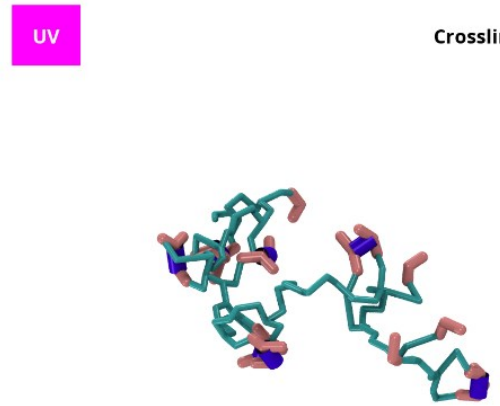

5.5 MD movie for folding of an individual conformer

A movie illustrating a single conformer of **P1** subjected to consecutively darkness, blue light, and UV light is included (Movie S1). As is shown in the snapshot, on the top-left corner the lighting stage is indicated when the total number of crosslinks is indicated on the top-right corner. For the polymer, the MMA backbone along with the linker segment towards styrylpyrene is colored as cyan, whereas the 3-component styrylpyrene is shown in pink color; intramolecular crosslinks are shown in dark blue with size-reinforced symbols. The size of the macromolecule is calculated through radius of gyration.

Along the MD trajectory, fluctuation of the molecular size is pronounced while the fluctuation in the number of crosslinks is much less, indicating the timescale separation between bond recombination and diffusion. The 3 distinguished exposure is equally divided in the movie. In the dark, for the first 1/3 of the movie, no bond recombination is present, the size of the polymer coil does not subject to constraint from crosslinks. Under blue light, for the middle 1/3 of the movie, irreversible crosslinking start to constrain the diffusion process and the degree of crosslink increases monotonically. As more crosslinks are formed with time, the polymer sees compaction. Exposed to UV light, for the latter 1/3 of the movie, reversible crosslinking reorganizes the conformer, where both number of crosslinks and the molecular size fluctuate accordingly. Across an ensemble of individual trajectories, there is statistically a slight expansion of the polymer chain under UV light compared to blue light condition, while the final photostationary state remains more compact than the free polymer coil.

5.6 Results for polymer P1'

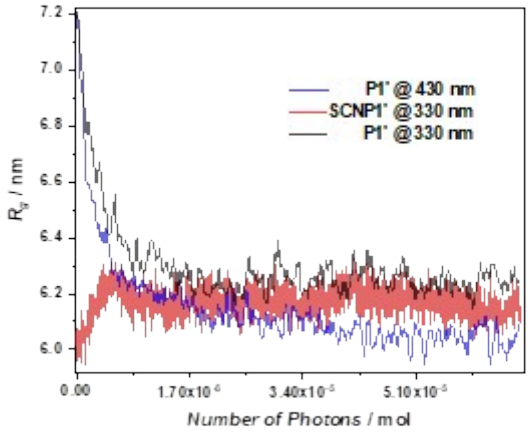

Figure S12: Simulated evolution of the R_g of **P1'/SCNP1'** under irradiation at different wavelength**.**

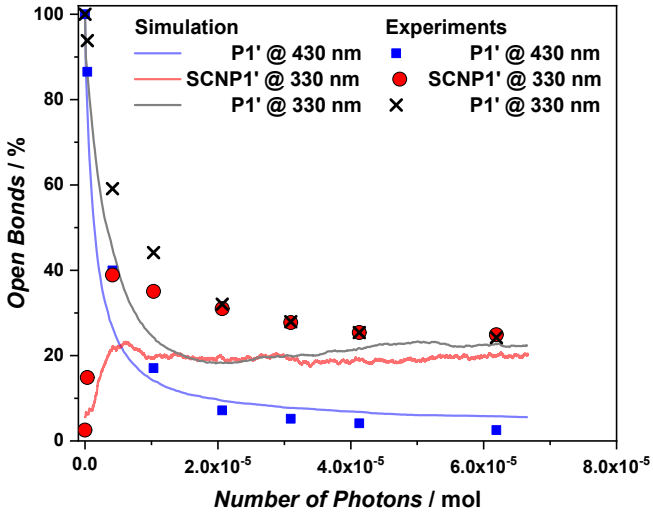

Figure S13: Comparison of the experimental and simulated number of photoreactive bonds in **P1'/SCNP1'** under irradiation at different wavelength.

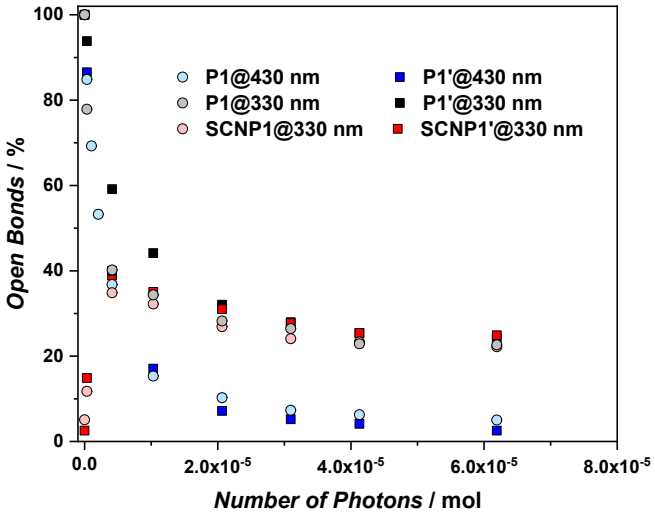

Figure S14: Comparison of the experimental number of photoreactive bonds in **P1'/SCNP1'**and **P1'/SCNP1'** under irradiation at different wavelength. The most significant difference between the two polymers can be observed at short irradiation times (*n* photons < 1 x10^{-5} mmol) of UV light irradiation of **P1** and **P1'**. The slower bond closing of the longer **P1'** in agreement with the simulations (compare Figure S12 and Figure 5).

6. References

[1] Frisch, H., Menzel, J.P., Bloesser, F.R., Marschner, D.E., Mundsinger, K., Barner-Kowollik, C., *J. Am. Chem. Soc.* ***2018***, *140*, 9551–9557.

[2] Fulmer, G.R., Miller, A.J.M., Sherden, N.H., Gottlieb, H.E., Nudelman, A., Stoltz, B.M., Bercaw, J.E., Goldberg, K.I., *Organometallics* ***2010***, *29*, 2176–2179.

[3] Fast, D.E., Lauer, A., Menzel, J.P., Kelterer, A.-M., Gescheidt, G., Barner-Kowollik, C., *Macromolecules* ***2017***, *50*, 1815–1823.

[4] Tuten, B.T., Menzel, J.P., Pahnke, K., Blinco, J.P., Barner-Kowollik, C., *Chem. Commun.* ***2017***, *53*, 4501–4504.

[5] Menzel, J.P., Noble, B.B., Lauer, A., Coote, M.L., Blinco, J.P., Barner-Kowollik, C., *J. Am. Chem. Soc.* ***2017***, *139*, 15812–15820.

[6] Marschner, D.E., Frisch, H., Offenloch, J.T., Tuten, B.T., Becer, C.R., Walther, A., Goldmann, A.S., Tzvetkova, P., Barner-Kowollik, C., *Macromolecules* ***2018***, *51*, 3802–3807.

[7] Groot, R.D., Warren, P.B., *J. Chem. Phys.* ***1997***, *107*, 4423–4435.

[8] Hoogerbrugge, P.J., Koelman, J.M.V.A., *EPL (Europhysics Lett.* ***1992***, *19*, 155.

[9] Smiatek, J., Allen, M.P., Schmid, F., *Eur. Phys. J. E* ***2008***, *26*, 115–122.

[10] Kremer, K., Grest, G.S., *J. Chem. Phys.* ***1990***, *92*, 5057–5086.

[11] Sirk, T.W., Slizoberg, Y.R., Brennan, J.K., Lisal, M., Andzelm, J.W., *J. Chem. Phys.* ***2012***, *136*, 134903.

[12] Plimpton, S., *J. Comput. Phys.* ***1995***, *117*, 1–19.